541
NACA TN 2115

TECH LIBRARY KAFB, NM
0065437

NATIONAL ADVISORY COMMITTEE FOR AERONAUTICS

TECHNICAL NOTE 2115

THEORETICAL WAVE DRAGS AND PRESSURE DISTRIBUTIONS FOR AXIALLY SYMMETRIC OPEN-NOSE BODIES

By John R. Jack

Lewis Flight Propulsion Laboratory
Cleveland, Ohio

Washington
June 1950

AFMTC
TECH
AFL 2811

TECH. LIBRARY KAFB, NM
0065437

NATIONAL ADVISORY COMMITTEE FOR AERONAUTICS

TECHNICAL NOTE 2115

THEORETICAL WAVE DRAGS AND PRESSURE DISTRIBUTIONS FOR AXIALLY SYMMETRIC OPEN-NOSE BODIES

By John R. Jack

SUMMARY

The variations of pressure distributions and coefficients of wave drag with fineness ratio, Mach number, and area ratio were calculated from linearized theory for a variety of open-nose bodies of revolution at zero angle of attack. Pressure distributions and values of wave-drag coefficients are given for several bodies with curved and straight lips and for design and off-design conditions including the effects of additive drag.

A comparison between the source method and the linearized method of characteristics showed that, for a given accuracy, computations by the source method were considerably faster; consequently, this method was used to compute the pressure distributions for all bodies investigated.

INTRODUCTION

Although methods for computing the supersonic flow over open-nose bodies of revolution have been known for some time (references 1 and 2), application of these methods has been limited to isolated cases. An investigation was therefore undertaken at the NACA Lewis laboratory to study systematically the variations of external pressure distributions and wave drags with fineness ratio, Mach number, and area ratio. The results presented herein are intended to serve as a guide in the design of external contours for supersonic nose inlets and to provide a basis for estimating the wave drag to be expected from such inlets. An evaluation of the relative merits of several methods of computation is also included.

SYMBOLS

The following symbols are used in this report:

A	local area of cowling
A_0/A_3	ratio of free-stream inlet area to maximum area
a	free-stream velocity of sound
C_D	coefficient of wave drag, drag/q_0A_0
C_p	pressure coefficient, $p-p_0/q$
D	maximum diameter of body
f_1,f_2	functions of $x/\beta R_N$
L	length of body
L/D	fineness ratio
M_0	free-stream Mach number, U/c
p	static pressure
q	dynamic pressure, $\frac{1}{2}\rho W^2$
R	radius of body
U	free-stream velocity
u	axial-velocity increment
v	radial-velocity increment
W	total velocity
x,r,θ	cylindrical coordinates
α_m	Mach angle, $\sin^{-1}\frac{1}{M_0}$
β	cotangent of $\alpha_m, \sqrt{M_0^2-1}$

1288

γ	ratio of specific heats of air, 1.4
ϵ	inclination of conical cowling with respect to free-stream direction
ϵ'	transformed cowling angle, $\beta \tan \epsilon = \tan \epsilon'$
θ	flow angle
θ_c	half-angle of cone
θ_l	cowling positioning angle, angle between axis of inlet and straight line connecting vertex of cone with lip of cowling
θ_s	shock angle
ρ	density

Subscripts:

0	free-stream conditions
3	station of maximum diameter
A,B,C,E	characteristic grid points
N	nose of body

BODIES AND VARIABLES INVESTIGATED

The bodies investigated are shown in figure 1. Most of the computations were made for conical cowlings (fig. 1(a)) to obtain the effect of free-stream Mach number M_0, area ratio A_0/A_3, and fineness ratio L/D. The ranges of the variables investigated for the conical cowlings were: Mach number, 1.5 to 2.5; area ratio, 0.400 to 0.800; and fineness ratio, 4 to 10. The effect of body contour on the pressure distribution and the wave drag for a Mach number of 2.0 was determined by investigating the flow over the curved cowlings (fig. 1(b)). Bodies for which the shock wave from the central body passes upstream of the cowling lip (fig. 1(c)) were considered in order to obtain the effect of additive drag for a free-stream Mach number of 2.0. (The additive drag, as defined by Ferri and Nucci, is the integral of the pressure coefficient along the bounding streamline between the conical

shock and the cowling lip.) Pressure distributions were also calculated as a function of Mach number for a conical cowling with a central body. This central body was so located that the conical shock intersected the upstream edge of the cowling at a Mach number of 2.0.

1288

COMPUTATIONAL METHODS

Three of several methods available for calculating the pressure distributions over open-nose bodies of revolution are considered: (1) the linearized source-distribution method (reference 1); (2) the rotational method of characteristics (reference 2); and (3) the method of linearized characteristics (suggested in references 3 and 4). A method applicable to conical cowlings has also been developed in reference 5. The method was not included in this investigation, however, because in addition to the usual restriction to small slopes, the method requires that the cowling be nearly cylindrical.

The method of linearized characteristics, for which the equations are derived in appendix A, will converge to the result given by the source method but the computing time for a specified accuracy is considerably greater (appendix B); therefore the source method was used to compute the remaining pressure distributions. The rotational method of characteristics is the most accurate but the computations are more lengthy than those required for the linearized methods. The linearized theories give satisfactory results except for the cases where the Mach number or the body slopes are large.

The wave-drag coefficient of each inlet was obtained by graphically integrating the pressure-coefficient distribution over the body surface. This coefficient was based on the free-stream inlet area and was defined by

$$C_D = \frac{\text{drag}}{q_0 A_0}$$

$$= \int C_p \, d\left(\frac{A}{A_0}\right)$$

L288

where

$$C_p = \frac{p-p_0}{q_0} = \frac{2}{\gamma M_0^2}\left(\frac{p}{p_0} - 1\right)$$

$$= \frac{2}{\gamma M_0^2}\left\{\left[1 - \frac{\gamma-1}{2}\left(2M_0\frac{u}{a} + \frac{u^2+v^2}{a^2}\right)\right]^{\frac{\gamma}{\gamma-1}} - 1\right\}$$

and A is the local area of the cowling.

RESULTS AND DISCUSSION

Conical cowlings. - The variations of pressure distribution in the axial direction for the conical cowlings are given in figure 2 for selected values of the cowling angle and free-stream Mach number. In each case, the pressure coefficient has the Ackeret value at the lip, decreases rather rapidly, and at large distances downstream becomes asymptotic to the surface value predicted for a cone of half-angle ϵ. The variations of pressure distribution with fineness ratio and area ratio may be obtained by the correlation of the cowling angle with area ratio and fineness ratio (fig. 3). The local pressures increase with increasing Mach number and decrease with increasing fineness ratio or area ratio.

If a first-order approximation for the pressure coefficient

$$C_p = \frac{p-p_0}{q_0} = -2\frac{u}{U}$$

is used and if an appropriate change of variable in the axially symmetric, linearized potential equation is made, the quantity $\beta^2 C_p$ becomes independent of Mach number. By use of this approximation the results in figure 4 are obtained, where $\beta^2 C_p$ is given as a function of the axial station $x/\beta R_N$ for various values of the transformed cowling angle ϵ'.

In obtaining the curves presented in figure 4, the quantity $\beta^2 C_p$ was found to vary almost linearly with ϵ' for small

values of $x/\beta R_N$. For larger values of $x/\beta R_N$ the variation of $\beta^2 C_p$ with ϵ' approached that of the cone solution, that is, $(\epsilon')^2 \log_e \epsilon'$. This behavior suggested an attempt to fit the curves with an equation of the form

$$\beta^2 C_p = f_1 \epsilon' - f_2 (\epsilon')^2 \log_e \epsilon' \qquad (1)$$

where ϵ' is given in radians and f_1 and f_2 are functions of $x/\beta R_N$. The values of f_1 and f_2 at $x/\beta R_N$ equal to zero can be immediately determined from the fact that the pressure coefficient at the lip is equal to the Ackeret value, $C_p = 2\epsilon/\beta$. Within the limitations of linearized theory and with $\beta \tan \epsilon = \tan \epsilon'$, the expression for the pressure coefficient at $x/\beta R_N = 0$ becomes $\beta^2 C_p = 2\epsilon'$. Thus at the cowling lip, f_1 must equal 2 and f_2 must equal 0. When the remaining values of f_1 and f_2 were obtained by matching the curves of $\beta^2 C_p$ plotted against ϵ' at two points, equation (1) described the curves of $\beta^2 C_p$ plotted against ϵ' accurately. As indicated by the preceding discussion, the term containing f_1 in equation (1) is the predominating term near the lip and the term containing f_2 predominates at large values of $x/\beta R_N$. This fact is shown in figure 5 where the functions f_1 and f_2 are plotted for values of $x/\beta R_N$ from 0 to 10. It is expected that equation (1) may be used over the range of ϵ' for which the linearized theory is valid. By use of equation (1), the general expression for the coefficient of wave drag of conical cowlings becomes

$$\beta^2 C_D = 2(\epsilon')^2 \int_0^{L/\beta R_N} (f_1 - f_2 \epsilon' \log_e \epsilon')(1 + \epsilon' t)\, dt \qquad (2)$$

where $t = x/\beta R_N$. This expression was not used to compute the coefficients of wave drag because pressure distributions were separately calculated. If pressure distributions are not available, however, the coefficient of wave drag can be obtained directly from equation (2).

By integrating the pressure distributions of figure 2 over the body surfaces, the variations of wave-drag coefficient with fineness ratio, Mach number, and area ratio are obtained (figs. 6 to 8, respectively). The coefficient of wave drag decreases as fineness ratio, Mach number, or area ratio increases.

1288

The variation of the coefficient of wave drag with Mach number is relatively small compared with the variation with fineness ratio or area ratio.

Although the wave drag decreases with an increase in fineness ratio, the friction drag increases. For large fineness ratios, the friction drag becomes the predominant part of the total drag; hence to obtain an optimum cowling this fact must be taken into account.

Additive drag and off-design conditions. - The coordinates and contours of the inlets used to investigate the effects of additive drag are given in figure 9. The curves were arbitrarily chosen, except that the lip of each body is faired into a streamline of the conical field produced by the central body. The design parameters for the bodies are

Free-stream Mach number, M_0	2.0
Area ratio, A_0/A_3	0.539
Fineness ratio, L/D	4.0
Cone half-angle, θ_c, deg	25

The linearized pressure distributions for the three inlets having cowling positioning angles of 32°, 36°, and 40° are shown in figure 10. The linearized coefficients of wave drag for these bodies, the coefficients of additive drag obtained from linearized theory, and the coefficients of additive drag obtained from exact conical flow theory are given in the following table with the coefficients of additive drag and body drag for a cylindrical body ($\theta_l = 30.5°$) and a conical body ($\theta_l = 42.6°$):

Cowling positioning angle, θ_l (deg)	Coefficient of wave drag, C_D (body)	Coefficient of additive drag $C_{D,a}$	
		Linearized cone theory	Exact cone theory
30.5	0	-----	0.381
32	.016	0.134	.257
36	.029	.046	.088
40	.018	.012	.020
42.6	.014	0	0

The linearized coefficients of wave drag for the bodies were computed by considering the bounding streamline between the conical shock and the cowling lip as part of the bodies; consequently, these

coefficients may be somewhat in error because the slope at any point of the bounding streamline is large. The coefficient of total drag (not including a skin-friction coefficient) is the sum of the coefficients of body and additive drag. Comparison of the coefficient of maximum total drag ($\theta_l = 30.5^\circ$, cylindrical cowling) with the coefficient of minimum total drag ($\theta_l = 42.6^\circ$, conical cowling) shows that in this case the coefficient of total wave drag may be reduced by approximately 96 percent by eliminating the additive drag; therefore, as pointed out by Ferri and Nucci, the avoidance of this additive drag over a required range of free-stream Mach numbers is important in cowling design.

Illustrated in figure 11 are the variations of pressure distribution with Mach number for a cowling designed for a free-stream Mach number of 2.0. The area ratio of the conical cowling is 0.539, and the fineness ratio is 4.0. At the design Mach number, the conical central body with a half-angle of 25° produces a shock that intersects the lip. For each off-design Mach number, the inlet flow is supersonic inasmuch as the normal shock is assumed to remain inside the inlet. The cowling in each case starts at the axial station x/R_N of 0.159. The pressure distribution upstream of this point for a free-stream Mach number of 1.8 results in an additive drag, because for any Mach number below 2.0 the conical shock is upstream of the cowling lip. As the Mach number increases, the pressure ratios on the cowling become higher.

When the pressure distributions are integrated over the body to obtain the coefficients of wave drag and are plotted as a function of free-stream Mach number (fig. 12), it is found that the coefficient of wave drag decreases rapidly from its value at a Mach number of 1.8 to its value at a Mach number of 2.0 and decreases slowly for Mach numbers higher than 2.0. The coefficient of wave drag at a free-stream Mach number of 1.8 is approximately twice as great as that at a Mach number of 2.0; however, again the slope at any point of the bounding streamline is sufficiently large so that the drag coefficient obtained at a Mach number of 1.8 may be in error. For this reason, the accuracy of the dashed portion of the curve in figure 12 between Mach numbers of 1.8 and 2.0 is doubtful.

Nonconical bodies without additive drag. - The coordinates and the contours for the nonconical inlets are shown in figure 13. The design parameters are

Free-stream Mach number, M_0	2.0
Area ratio, A_0/A_3	0.539
Fineness ratio, L/D	4.0
Cone half-angle, θ_c, deg	25

The initial lip angle for contours 1, 2, and 3 is the same as the flow-deflection angle behind the conical shock emanating from the central body. The results may again be somewhat in error because of the large slopes of the lips; however, the linearized theory should predict the drag trends of these bodies.

Pressure distributions for the curved contours of figure 13 are compared with the conical-cowling pressure distribution in figure 14; the coefficients of wave drag for the four cowlings are presented in the following table:

Contour	Coefficient of wave drag C_D
1	0.089
2	.042
3	.040
4	.014

These values of the coefficient of wave drag changed appreciably with the external contour of the cowling and the desirability of producing a rapid flow expansion near the lip is indicated.

SUMMARY OF RESULTS

The computations of the theoretical supersonic wave drag of axially symmetric open-nose bodies at zero angle of attack may be summarized as follows:

1. For conical cowlings, the local pressures on a body increased with increasing Mach number and decreased with increasing fineness ratio and with area ratio. The coefficients of wave drag obtained from the pressure distributions decreased with increasing fineness ratio, Mach number, or area ratio.

2. In order to determine the effect of additive drag, a series of cowlings having a common central body and the same mass flows were investigated at a Mach number of 2.0. For these inlets, the least total drag was obtained with a conical cowling the leading edge of which was located at the shock from the central body. As the leading edge was moved downstream from this location, the drag of the cowling decreased, but the increase in additive drag was sufficient to overbalance this decrease.

3. For off-design conditions, the total wave drag increased rapidly as the shock from the central body passed upstream of the cowling lip. When this shock fell inside the lip, little change in wave-drag coefficient with Mach number was obtained.

4. At a Mach number of 2.0, the coefficients of wave drag obtained for the nonconical bodies without additive drag varied from 0.089 to 0.040. The magnitude of the drag depended on the rate of flow expansion in the vicinity of the cowling lip. For an immediate flow expansion, that is, a conical cowling, the coefficient of wave drag was 0.014.

Lewis Flight Propulsion Laboratory,
National Advisory Committee for Aeronautics,
Cleveland, Ohio, December 15, 1949.

L288

APPENDIX A

DERIVATION OF EQUATIONS FOR LINEARIZED METHOD OF CHARACTERISTICS

The linearized differential equation for supersonic flow is of hyperbolic form and therefore has real characteristics. The use of these characteristics for the numerical computation of supersonic flow fields when the perturbation velocities are small has been suggested by several authors. (See, for example, references 3 and 4.) Inasmuch as these characteristic equations are very simple to use for calculating axially symmetric flow, a comparison of this method with the source method was considered desirable. The required difference equations are derived herein.

For axially symmetric flow, the linearized equation for the perturbation velocities u and v is

$$\beta^2 \frac{\partial u}{\partial x} - \frac{\partial v}{\partial r} - \frac{v}{r} = 0 \tag{A1}$$

The characteristics of this equation are given by (reference 4)

$$\frac{dr}{dx} = \pm \frac{1}{\beta}$$

so that the total derivatives of the perturbation-velocity components become

$$\frac{du}{dx} = \frac{\partial u}{\partial x} \pm \frac{1}{\beta} \frac{\partial u}{\partial r} \tag{A2}$$

$$\frac{dv}{dx} = \frac{\partial v}{\partial x} \pm \frac{1}{\beta} \frac{\partial v}{\partial r} \tag{A3}$$

where the plus sign is used for family I and the minus sign is used for family II (fig. 15(a)). By solving equations (A2) and (A3) for $\partial u/\partial x$ and $\partial v/\partial r$ and by making use of the irrotationality condition, equation (A1) for family I becomes

$$du - \frac{1}{\beta} dv - \frac{1}{\beta^2} \frac{v}{r} dx = 0 \tag{A4}$$

When the grid shown in figure 15(a) is used, equation (A4) may be expressed in difference form as follows:

$$(u_C - u_A) - \frac{1}{\beta} (v_C - v_A) - \frac{1}{\beta^2} \left(\frac{v}{r}\right)_A (x_C - x_A) = 0$$

$$u_C - \frac{v_C}{\beta} = u_A - \frac{v_A}{\beta} + \frac{1}{\beta^2} \left(\frac{v}{r}\right)_A (x_C - x_A) = F_A$$

or

$$u_C = \frac{v_C}{\beta} + F_A \tag{A5}$$

Similarly, for family II, the difference equation is

$$u_C + \frac{v_C}{\beta} = u_B + \frac{v_B}{\beta} + \frac{1}{\beta^2} \left(\frac{v}{r}\right)_B (x_C - x_B) = F_B$$

or

$$u_C = - \frac{v_C}{\beta} + F_B \tag{A6}$$

By solving equations (A5) and (A6) simultaneously, u_C and v_C are found to be

$$u_C = \frac{1}{2} (F_A + F_B) \tag{A7}$$

$$v_C = \frac{\beta}{2} (F_B - F_A) \tag{A8}$$

The flow angle θ and the total velocity W are introduced by letting

$$u + U = W \cos \theta \tag{A9}$$

$$v = W \sin \theta \tag{A10}$$

1288

1288

From equations (A7) to (A10), the expressions for θ_C and W_C are found to be

$$\theta_C = \tan^{-1} \frac{\beta(G_B - G_A)}{G_B + G_A} \tag{A11}$$

$$W_C = \frac{\beta(G_B - G_A)}{2 \sin \theta_C} \tag{A12}$$

where

$$G_A = W_A \cos \theta_A \left[1 - \frac{\tan \theta_A}{\beta}\left(1 - \frac{x_C - x_A}{\beta r_A}\right)\right]$$

$$G_B = W_B \cos \theta_B \left[1 + \frac{\tan \theta_B}{\beta}\left(1 + \frac{x_C - x_B}{\beta r_B}\right)\right]$$

By considering figure 15(b), the expressions for the coordinates x_C and r_C may be derived as

$$x_C = \frac{1}{2}(x_B + x_A) + \frac{\beta}{2}(r_B - r_A) \tag{A13}$$

$$r_C = r_C - \frac{x_C - x_B}{\beta} = r_A + \frac{x_C - x_A}{\beta} \tag{A14}$$

For the velocity components at a body boundary point (fig. 15(c)), the difference equation is

$$u_E + \frac{v_E}{\beta} = u_C + \frac{v_C}{\beta} + \frac{1}{\beta^2}\left(\frac{v}{r}\right)_C (x_E - x_C) \tag{A15}$$

Inasmuch as the flow angle at the boundary is known, one of the unknown velocity components in equation (A15) can be eliminated with the aid of the boundary condition

$$\tan \theta_E = \frac{v_E}{U + u_E} \tag{A16}$$

By making the substitutions given in equations (A9) and (A10), W_E is found to be

$$W_E = W_C \frac{\cos \theta_C}{\cos \theta_E} \left[\frac{1 + \frac{\tan \theta_C}{\beta} \left(1 + \frac{x_E - x_C}{\beta r_C} \right)}{1 + \frac{\tan \theta_E}{\beta}} \right] \tag{A17}$$

With the velocity known, the static pressure at a boundary point is determined from

$$\frac{p_E}{p_0} = \left[1 - \frac{\gamma - 1}{2} M_0^2 \left(\frac{W_E^2}{W_0^2} - 1 \right) \right]^{\frac{\gamma}{\gamma - 1}} \tag{A18}$$

The coordinates x_E and R_E for the boundary points are

$$x_E = \frac{r_C - r_A + \frac{x_C}{\beta} + x_A \tan \theta_A}{\frac{1}{\beta} + \tan \theta_A} \tag{A19}$$

$$R_E = r_C - \frac{x_E - x_C}{\beta} \tag{A20}$$

The linearized method of characteristics differs from the exact method (reference 2) in that all characteristics are straight and parallel so that the characteristic grid can be constructed in advance of any computations. All the coordinates of the grid points are therefore known and need not be computed if a graphical representation is employed. The equations for the velocity components (equations (A12) and (A17)) are, of course, also considerably simpler than those obtained for the exact method of characteristics.

1288

APPENDIX B

COMPARISON OF ACCURACY AND COMPUTING TIME

A comparison of the pressure distributions computed by the linearized method of characteristics and by the source method is shown in figure 16. One curve was obtained with a spacing between boundary points of $\Delta x/R_N = 0.5$ and a second with $\Delta x/R_N = 0.125$. The third curve was obtained by the source method with 11 boundary points. It was found for the source-distribution method that any number of boundary points above 10 did not appreciably alter the pressure-distribution curve. The calculations by the method of linearized characteristics, as presented herein, require a larger number of boundary points than the source method. The asymptotic solution (corresponding to zero grid spacing), however, should be the same for the two methods inasmuch as both methods are derived from the same differential equation.

A comparison of the source method with the method of rotational characteristics is presented in figure 17 and shows a relatively large error in the vicinity of the cowling lip. The wave-drag coefficients obtained by integrating the pressure distributions of figure 17 to the point $x/R_N = 2$ are: exact-characteristics method, 0.100; and source method, 0.064. The magnitude of the error is approximately 36 percent and should represent a near maximum. Inasmuch as the initial flow deflection at the lip is large (15.5°), this error is to be expected because linearized theory is inaccurate for large angles. Some idea of the magnitude of the error due to the limitations of linearized theory (in regard to flow-deflection angles) can be obtained from figure 18, where the pressure coefficients obtained from linearized theory and from shock theory are plotted as functions of the lip or initial flow-deflection angle.

In making a calculation by the source method for a body having 15 boundary points (average number of points used in the calculations), the computing time, including the time required for checking the computations, was approximately 17 man-hours. If the number of boundary points was increased to 20, the time necessary for computing and checking would be 30 man-hours. The time to make the same calculation (curve with $\Delta x/R_N = 0.5$, fig. 16) by using the linearized method of characteristics was approximately 160 man-hours. This time, however, includes computing the coordinates of the grid points and could be shortened if these were read from the grid network. The same calculation

made by the method of characteristics for rotational flow required approximately 240 man-hours. The over-all time for a calculation by any one of the preceding methods depends, of course, on the experience of the computers and should not be considered a minimum value.

REFERENCES

1. Brown, Clinton E., and Parker, Hermon M.: A Method for the Calculation of External Lift, Moment, and Pressure Drag of Slender Open-Nose Bodies of Revolution at Supersonic Speeds. NACA Rep. 808, 1945. (Formerly NACA ACR L5I29.)

2. Ferri, Antonio: Application of the Method of Characteristics to Supersonic Rotational Flow. NACA Rep. 841, 1946. (Formerly NACA TN 1135.)

3. Moeckel, W. E.: Use of Characteristic Surfaces for Unsymmetrical Supersonic Flow Problems. NACA TN 1849, 1949.

4. Sauer, Robert: Introduction to Theoretical Gas Dynamics. J. W. Edwards (Ann Arbor), 1947, pp. 68-70.

5. Ward, G. N.: The Approximate External and Internal Flow past a Quasi-Cylindrical Tube Moving at Supersonic Speeds. Quarterly Jour. Mech. and Appl. Math., vol. 1, pt. 2, June 1948, pp. 225-245.

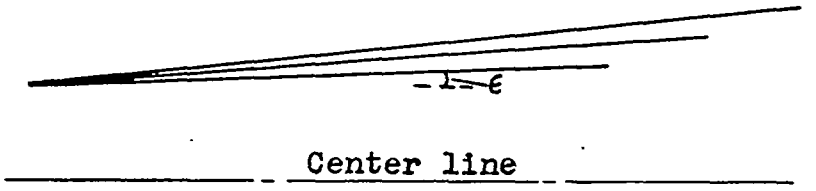

(a) Conical cowlings.

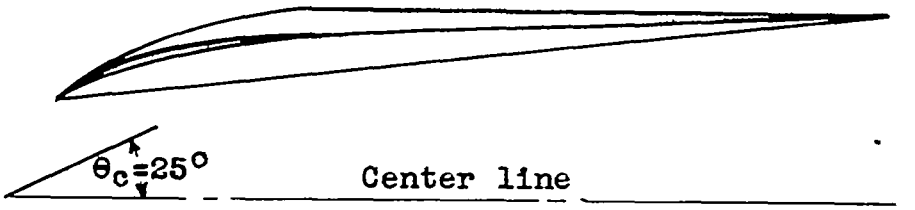

(b) Curved cowlings.

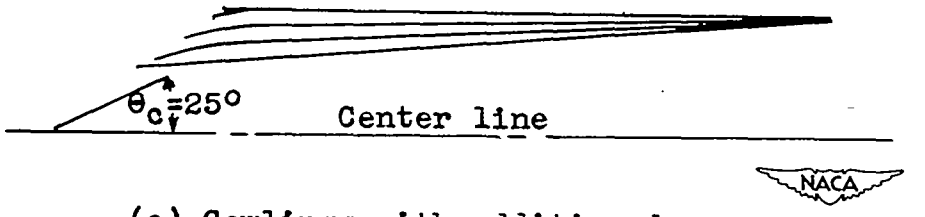

(c) Cowlings with additive drag.

Figure 1. - Bodies investigated.

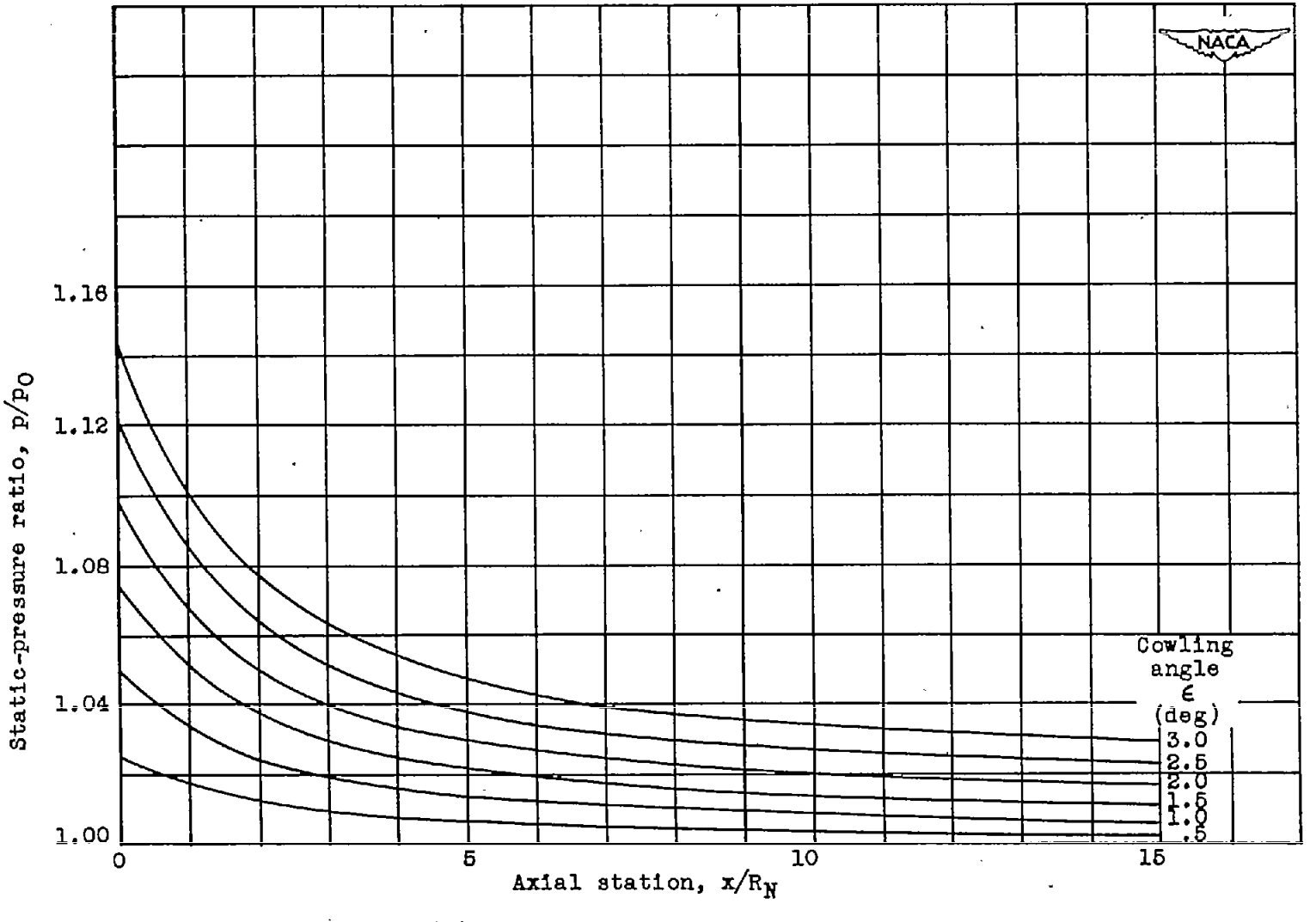

(a) Free-stream Mach number, 1.5.

Figure 2. - Pressure distributions in axial direction for conical cowlings.

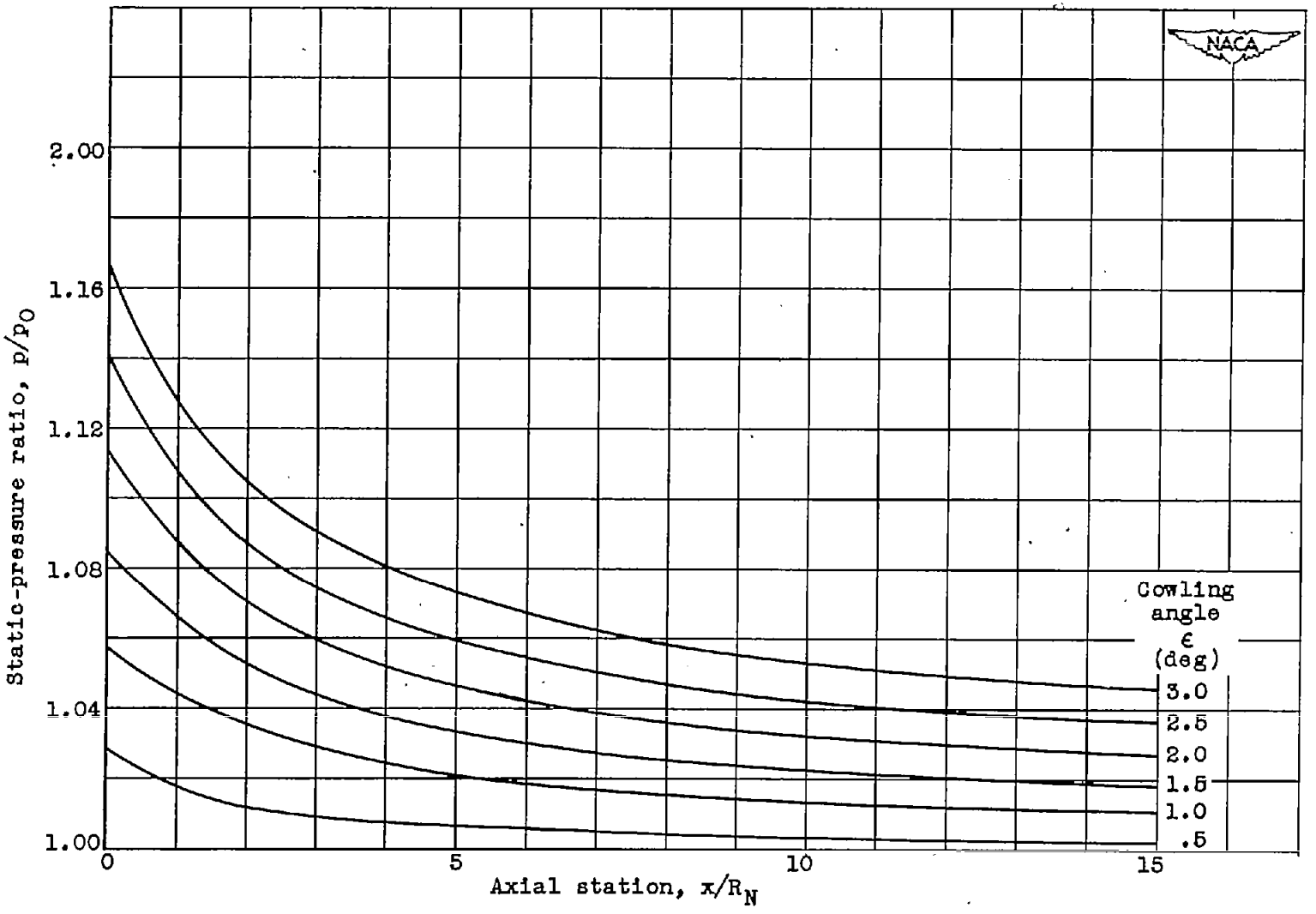

(b) Free-stream Mach number, 2.0.

Figure 2. - Continued. Pressure distributions in axial direction for conical cowlings.

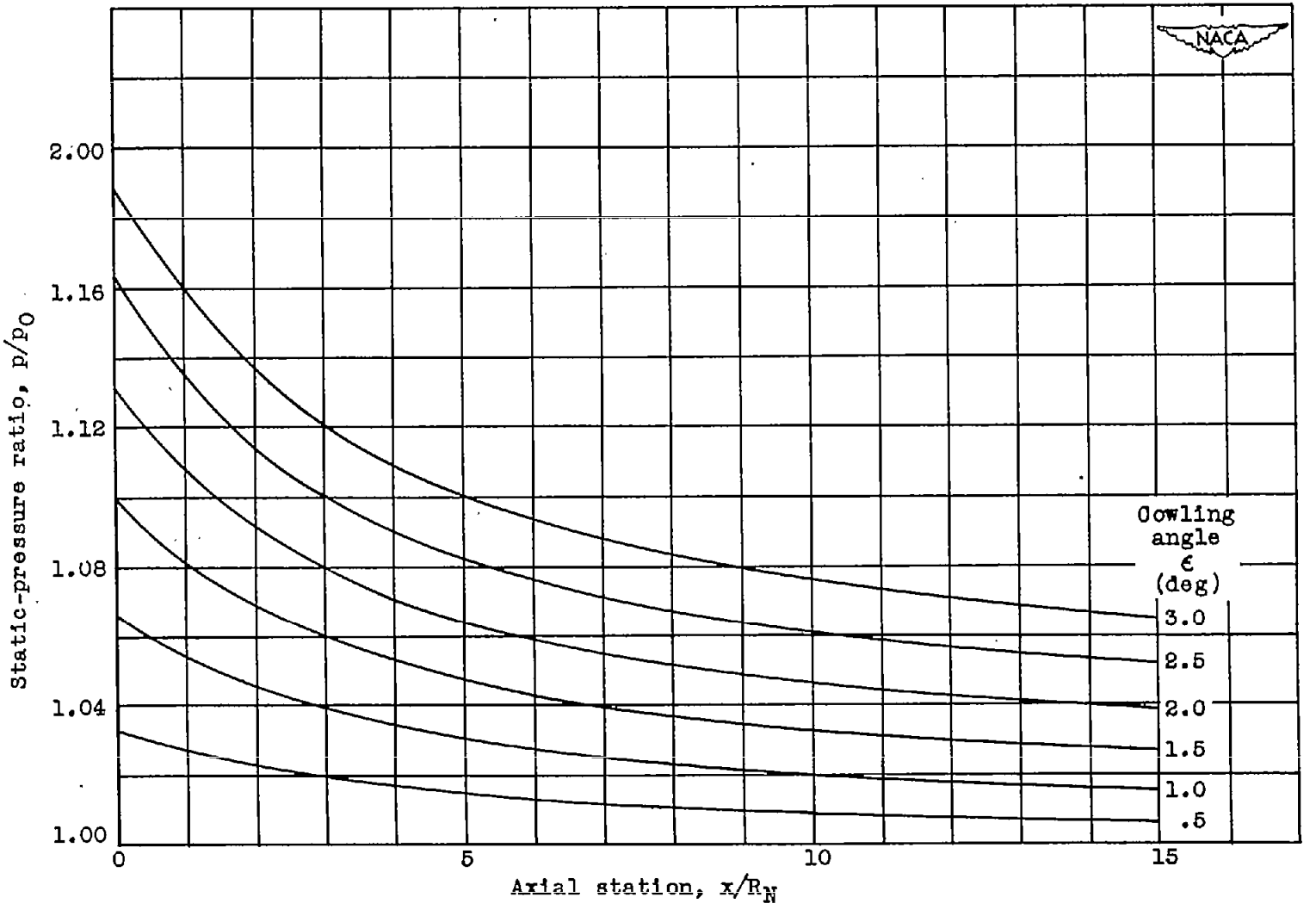

(c) Free-stream Mach number, 2.5.

Figure 2. - Concluded. Pressure distributions in axial direction for conical cowlings.

1288

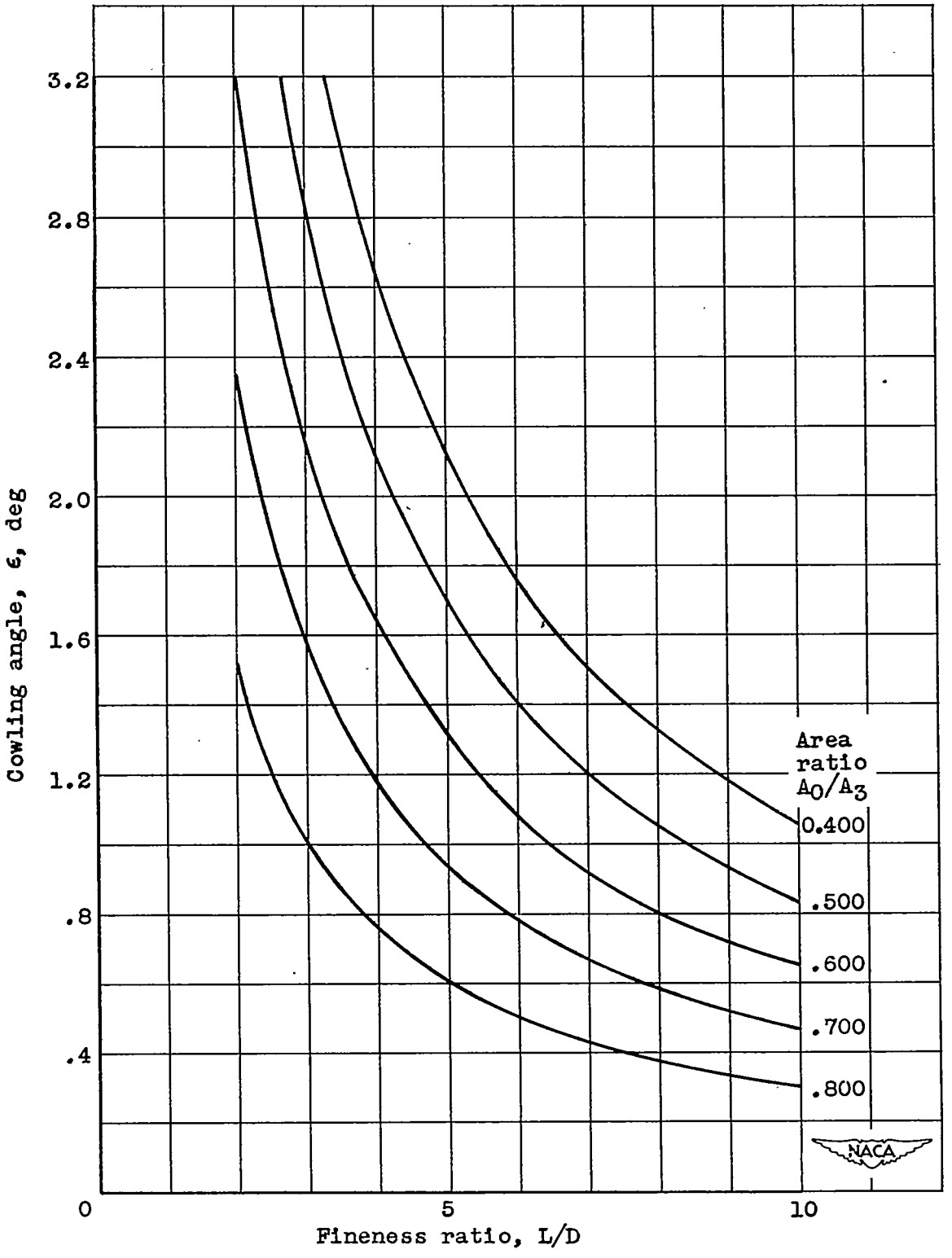

Figure 3. - Relations among cowling angle, fineness ratio, and area ratio.

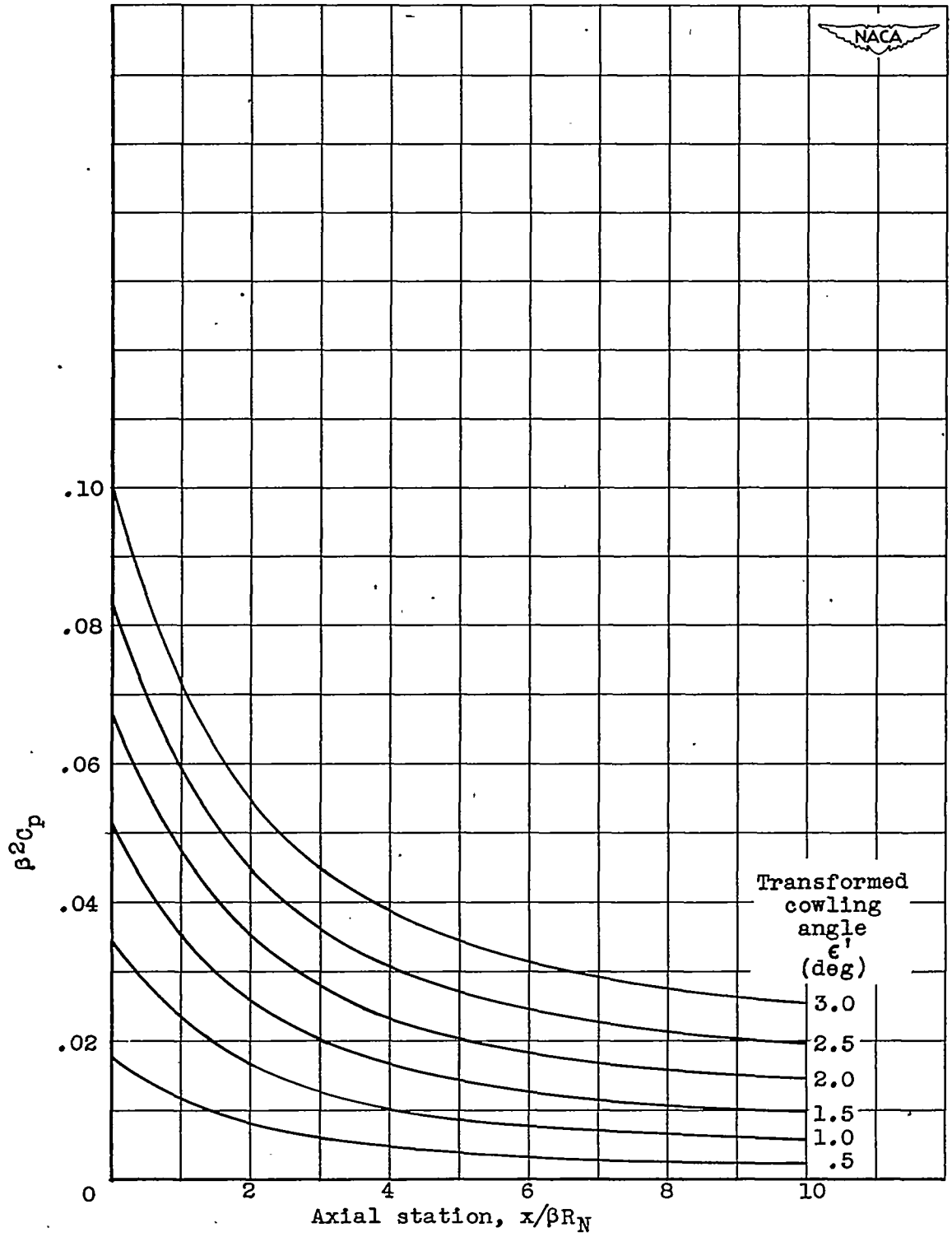

Figure 4. - Pressure distributions obtained from first-order equation for pressure coefficient. $\beta \tan \epsilon = \tan \epsilon'$.

1288

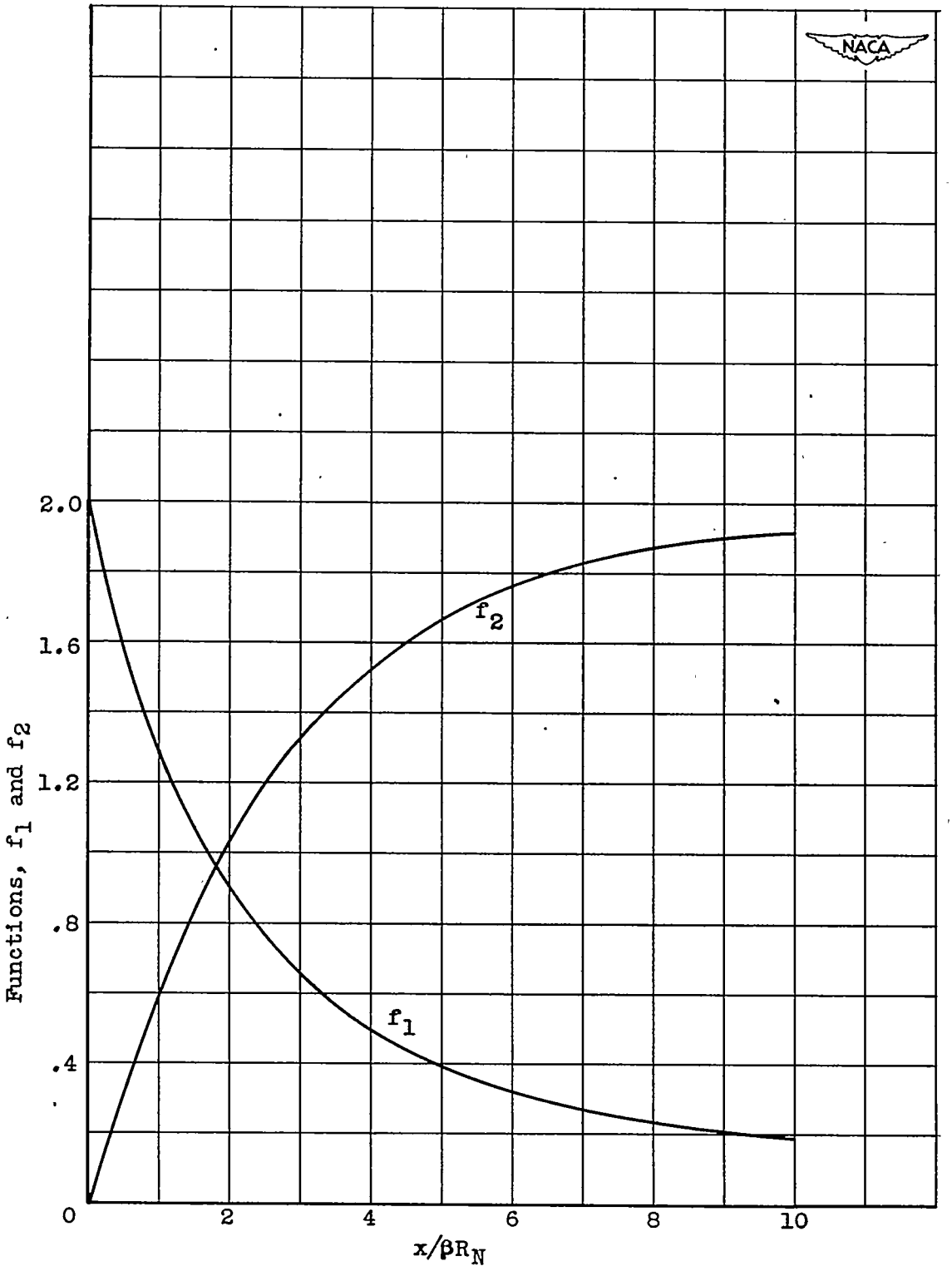

Figure 5. - Variation of functions of $x/\beta R_N$.

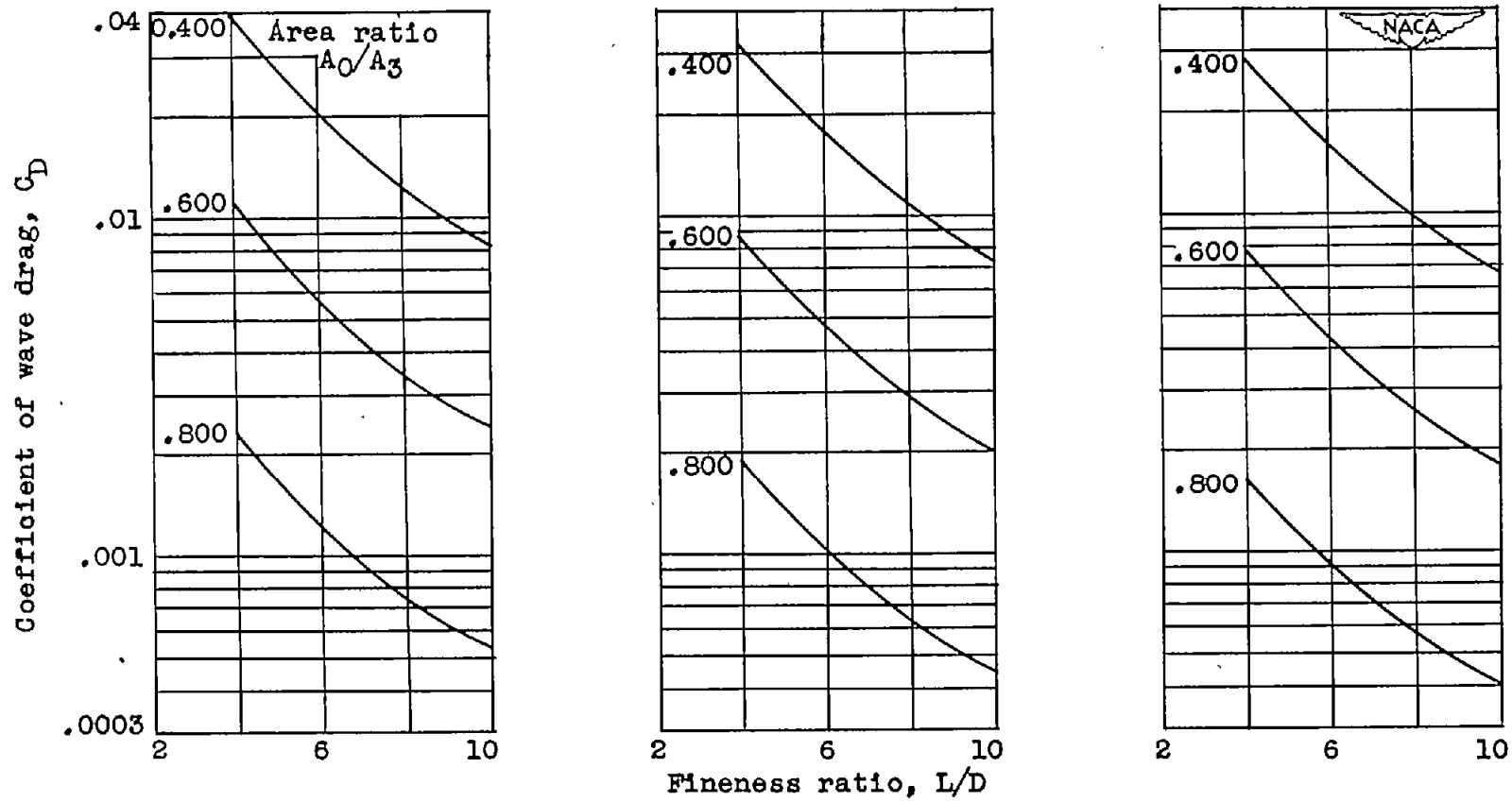

(a) Free-stream Mach number, 1.5.

(b) Free-stream Mach number, 2.0.

(c) Free-stream Mach number, 2.5.

Figure 6. - Variation of coefficient of wave drag with fineness ratio.

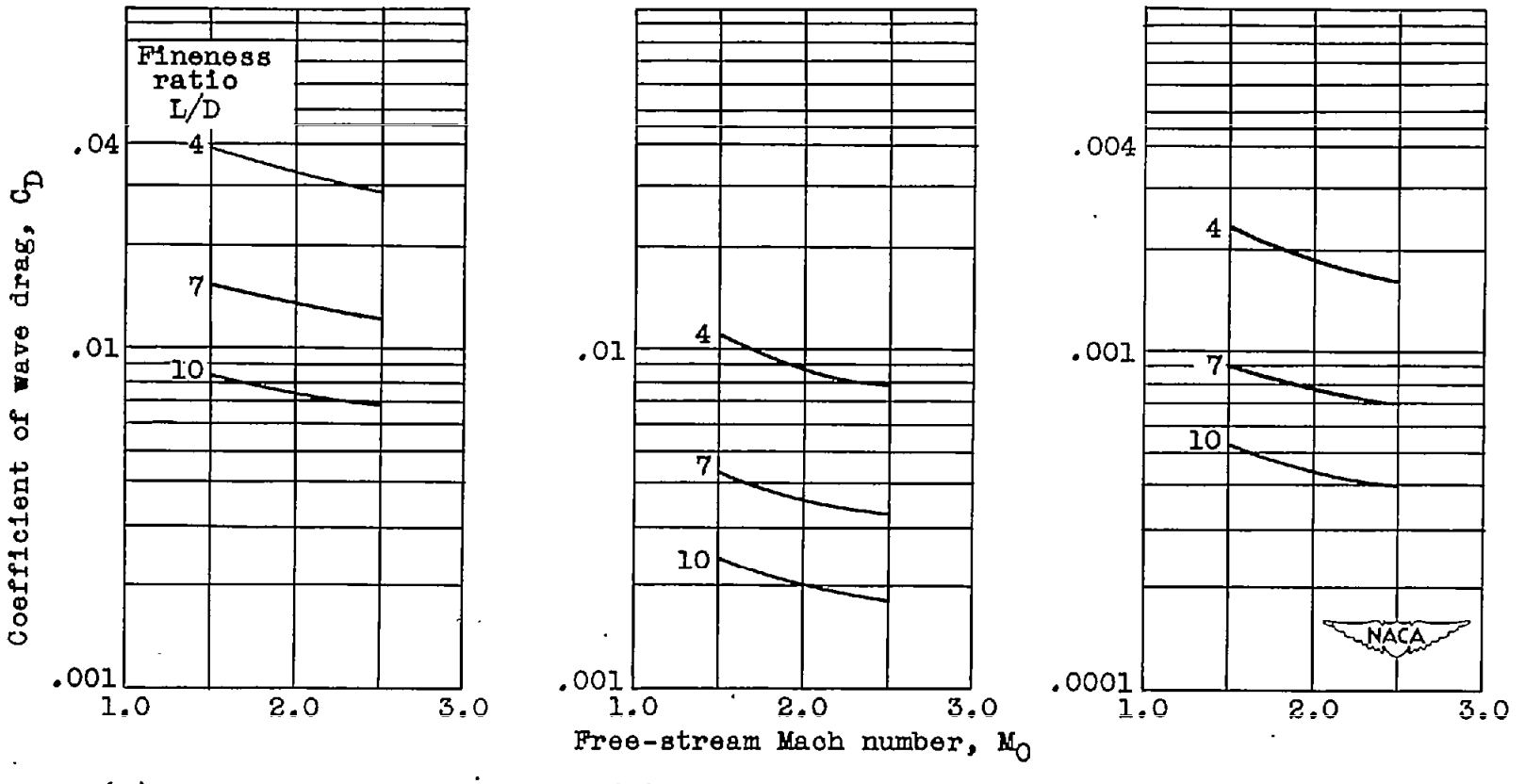

(a) Area ratio, 0.400. (b) Area ratio, 0.600. (c) Area ratio, 0.800.

Figure 7. - Variation of coefficient of wave drag with free-stream Mach number.

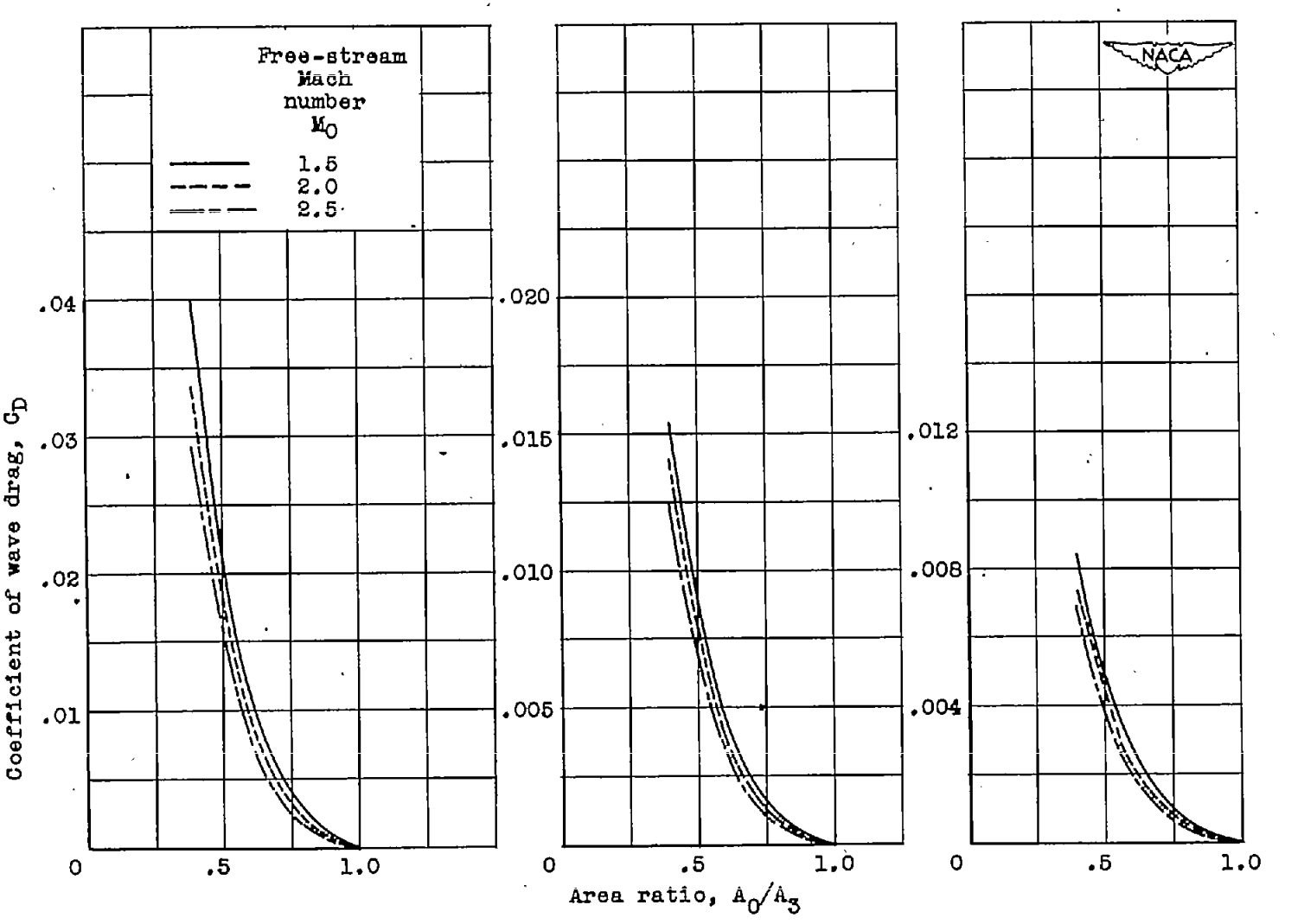

(a) Fineness ratio, 4.0. (b) Fineness ratio, 7.0. (c) Fineness ratio, 10.0.

Figure 8. - Variation of coefficient of wave drag with area ratio.

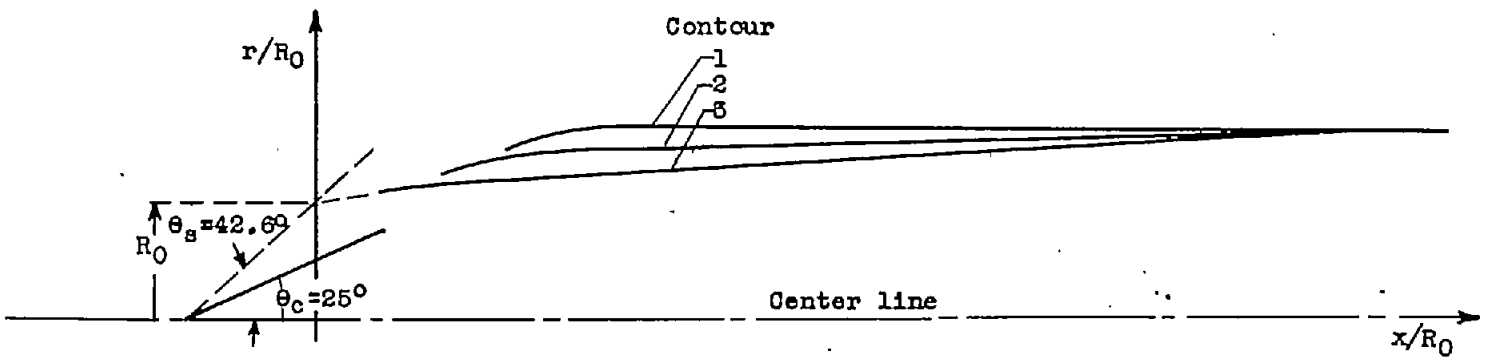

x/R_0	0.136	0.240	0.345	0.428	0.553	0.658	0.762	0.936	1.176	1.596	2.226	5.246	8.236	11.04	11.34	11.84
R_1/R_0	-----	-----	-----	-----	-----	-----	-----	1.260	1.310	1.350	1.360	1.360	1.360	1.360	1.360	1.360
R_2/R_0	-----	-----	-----	1.100	1.130	1.150	1.170	1.190	1.210	1.230	1.240	1.280	1.310	1.358	1.360	------
R_3/R_0	1.026	1.048	1.060	1.066	1.076	1.083	1.085	1.090	1.096	1.106	1.123	1.202	1.280	1.360	------	------

NACA

Figure 9. - Cowling inlets used to investigate effect of additive drag. Free-stream Mach number, 2.0; area ratio, 0.539; fineness ratio, 4.0; cone half-angle, 25°.

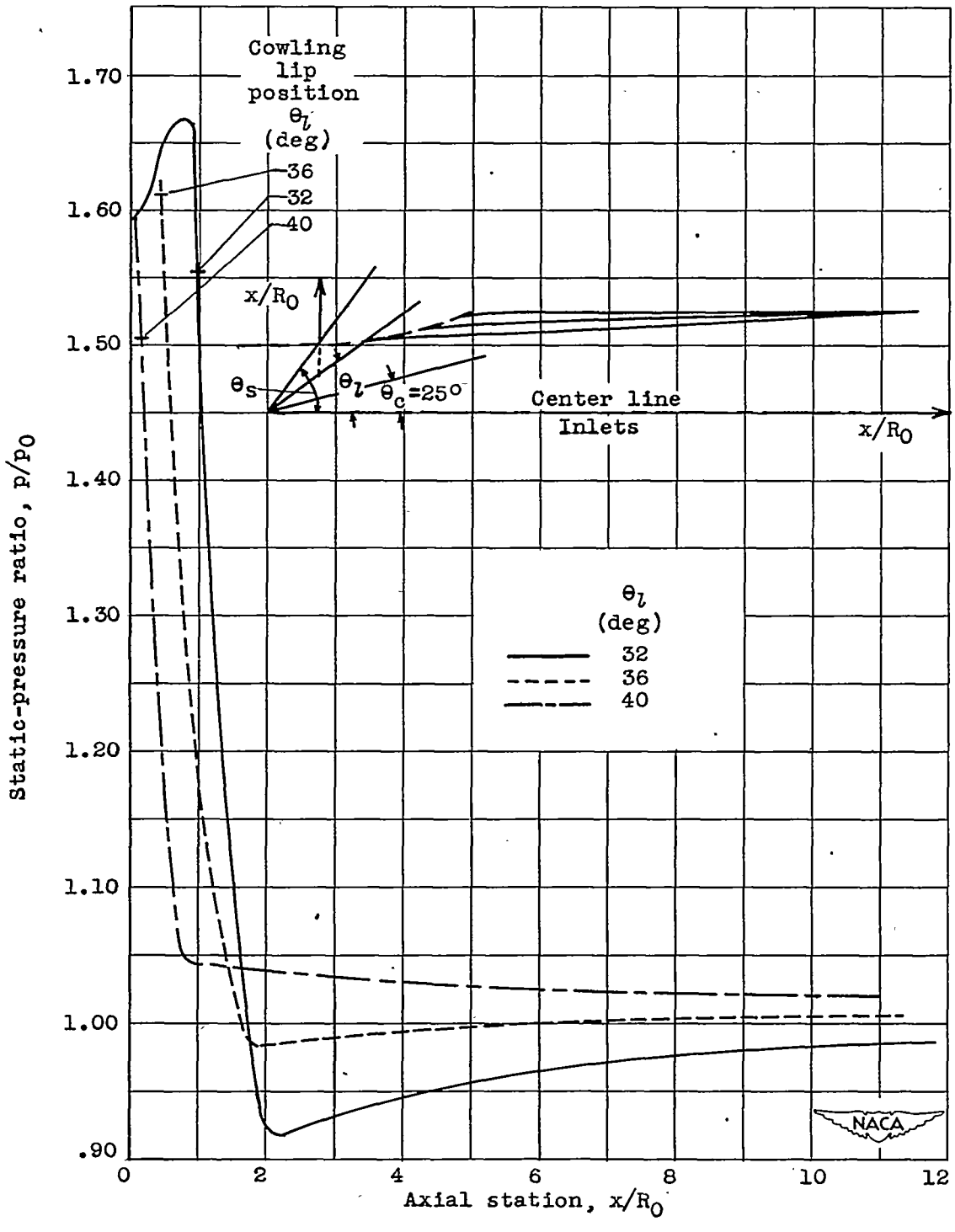

Figure 10. - Pressure distribution along bounding streamline and over body contour for inlets with additive drag. Free-stream Mach number, 2.0; area ratio, 0.539; fineness ratio, 4.0.

1288

1283

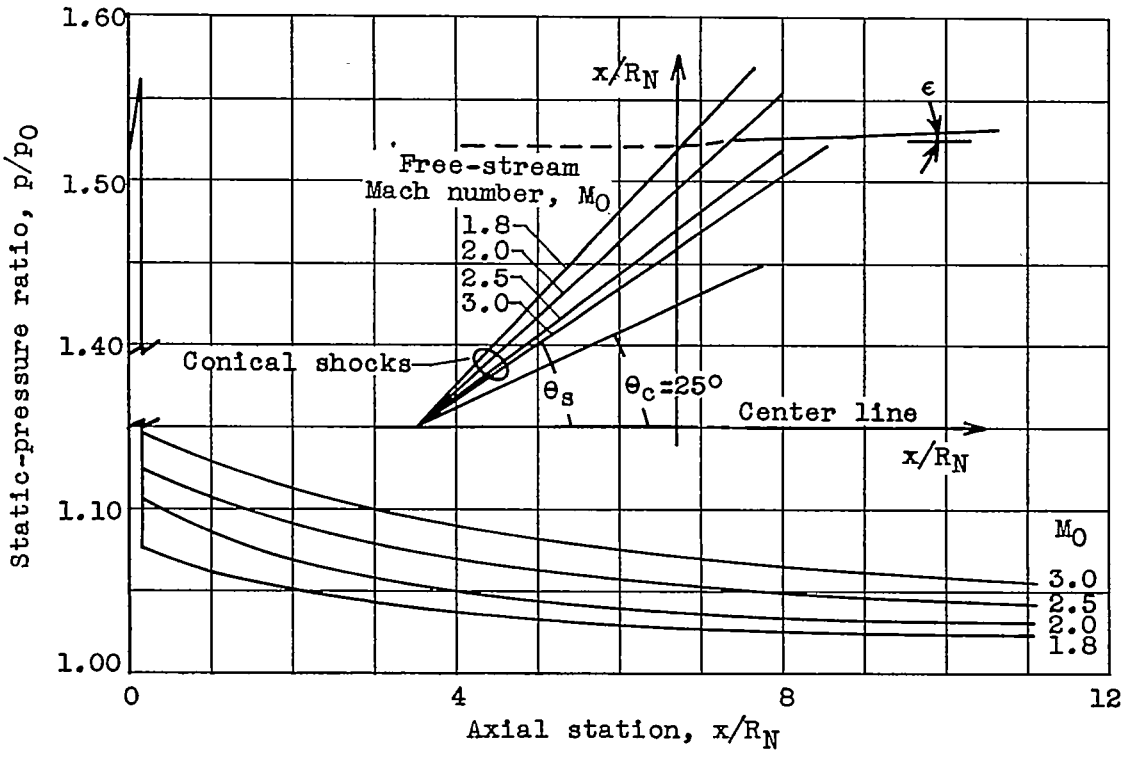

Figure 11. - Variation of pressure distribution with Mach number for a cowling designed for free-stream Mach number of 2.0. Area ratio, 0.539; fineness ratio, 4.0; cowling angle, 1.9°. Cowling in each case starts at $x/R_N = 0.159$.

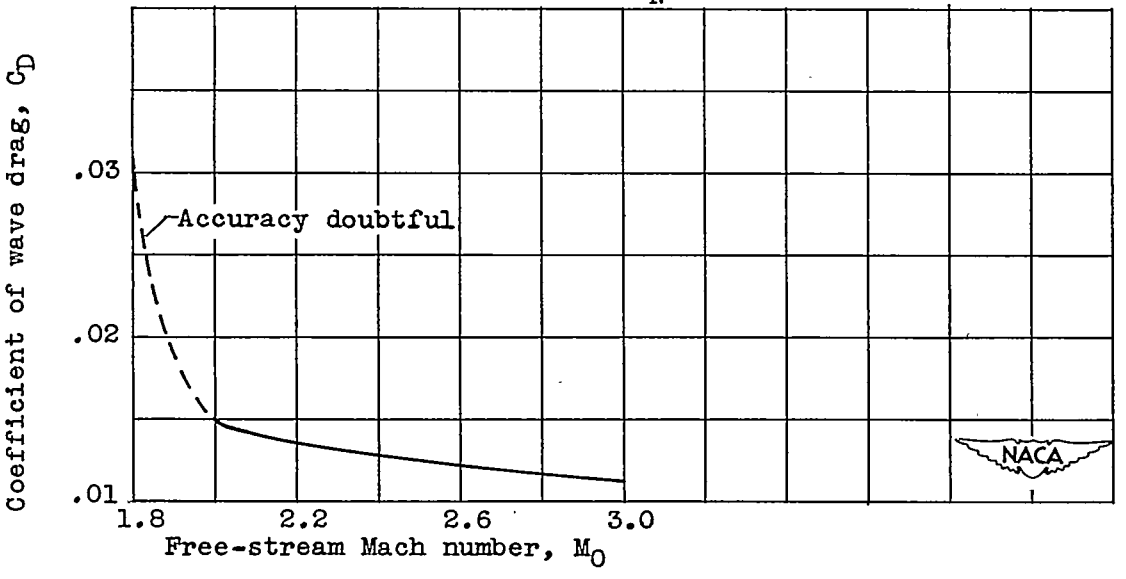

Figure 12. - Coefficient of wave drag as function of Mach number for nose inlet designed for free-stream Mach number of 2.0. Area ratio, 0.539; fineness ratio, 4.0.

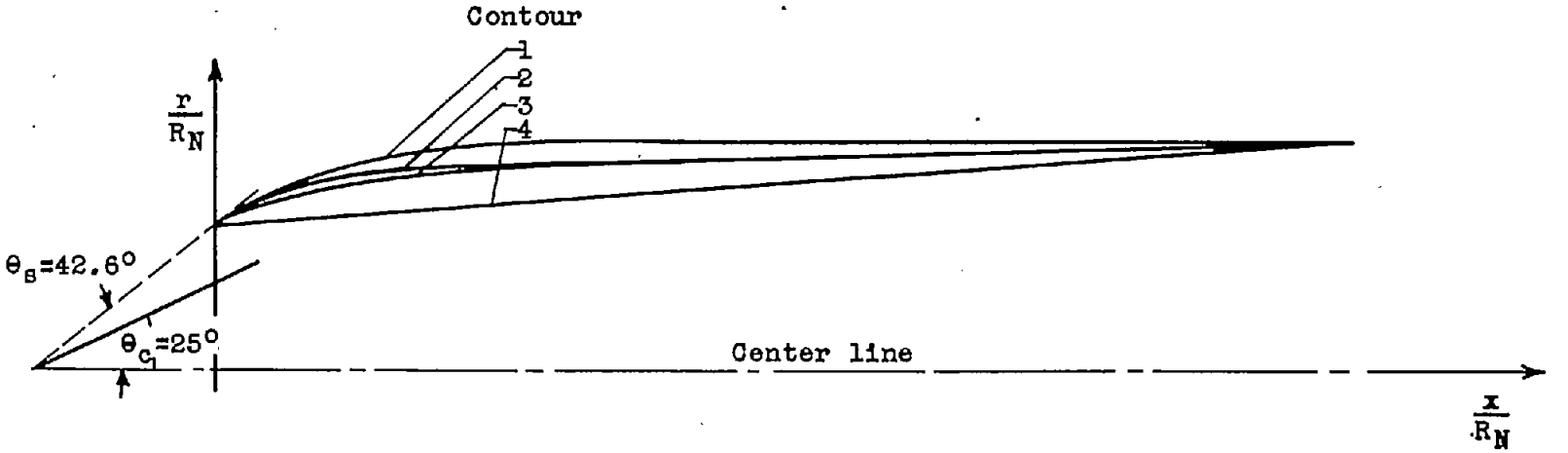

x/R_N	0	0.313	0.626	0.939	1.25	1.56	1.88	2.19	2.51	2.82	4.12	5.43	6.74	8.04	9.34	10.9
R_1/R_N	1	1.07	1.13	1.18	1.23	1.26	1.30	1.32	1.33	1.34	1.36	1.36	1.36	1.36	1.36	1.36
R_2/R_N	1	1.07	1.13	1.18	1.20	1.217	1.221	1.225	1.23	1.234	1.25	1.27	1.29	1.32	1.34	1.36
R_3/R_N	1	1.05	1.09	1.12	1.15	1.17	1.19	1.20	1.22	1.23	1.25	1.27	1.29	1.32	1.34	1.36

Figure 13. - Coordinates and contours for nonconical inlets. Free-stream Mach number, 2.0; area ratio, 0.539; fineness ratio, 4.0.

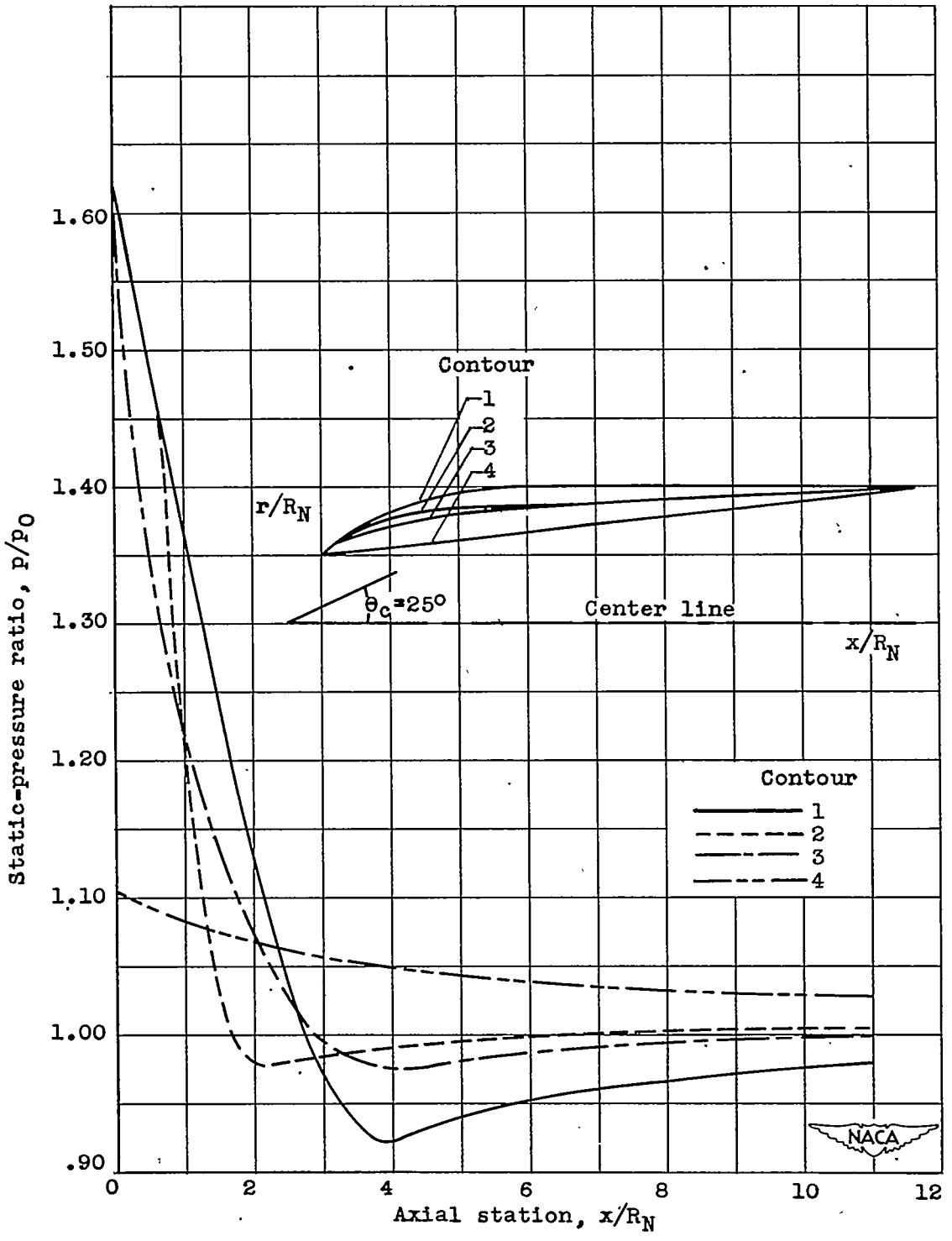

Figure 14. - Pressure distributions over several body contours. Free-stream Mach number, 2.0; area ratio, 0.539; fineness ratio, 4.0.

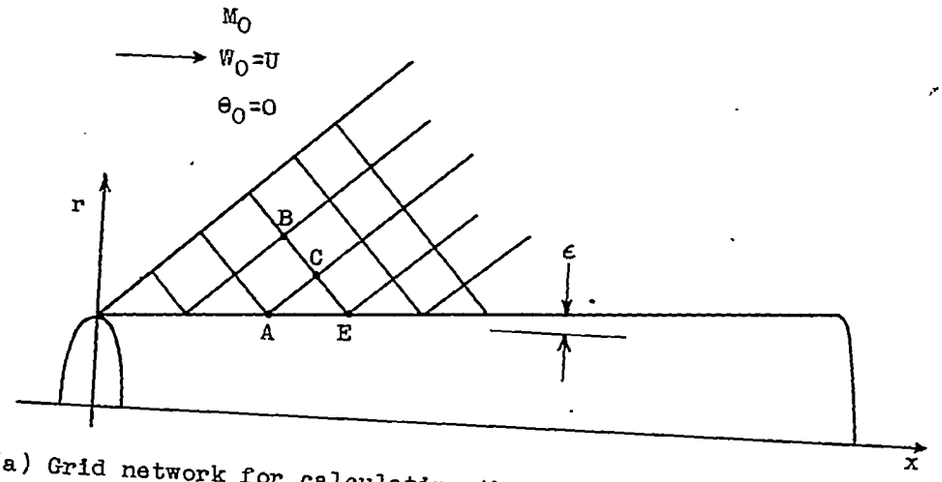

(a) Grid network for calculating the flow field for an open-nose body of revolution.

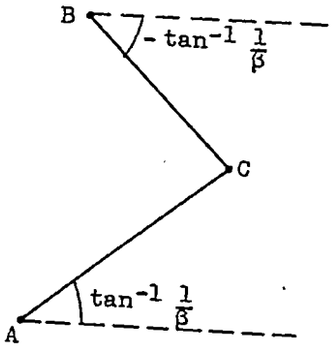

(b) Geometry of grid points.

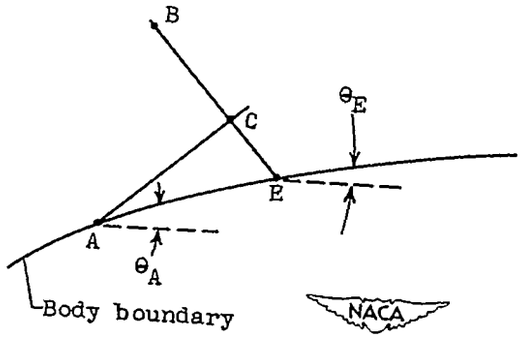

(c) Geometry of boundary points.

Figure 15. - Geometric relations between grid points and body boundary.

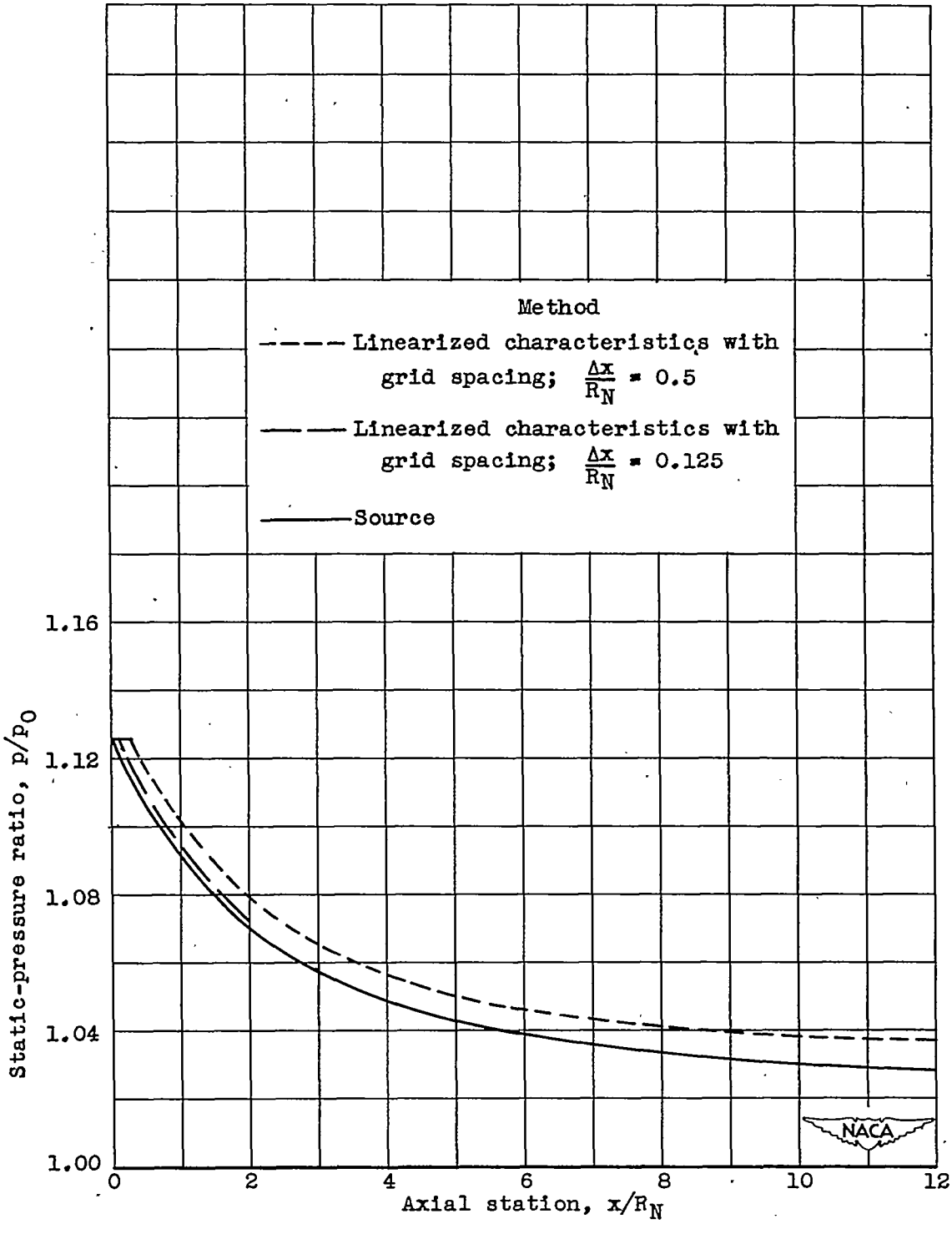

Figure 16. - Comparison of pressure distributions obtained with linearized characteristics and with source method. Free-stream Mach number, 1.5; area ratio, 0.393; fineness ratio, 4.0.

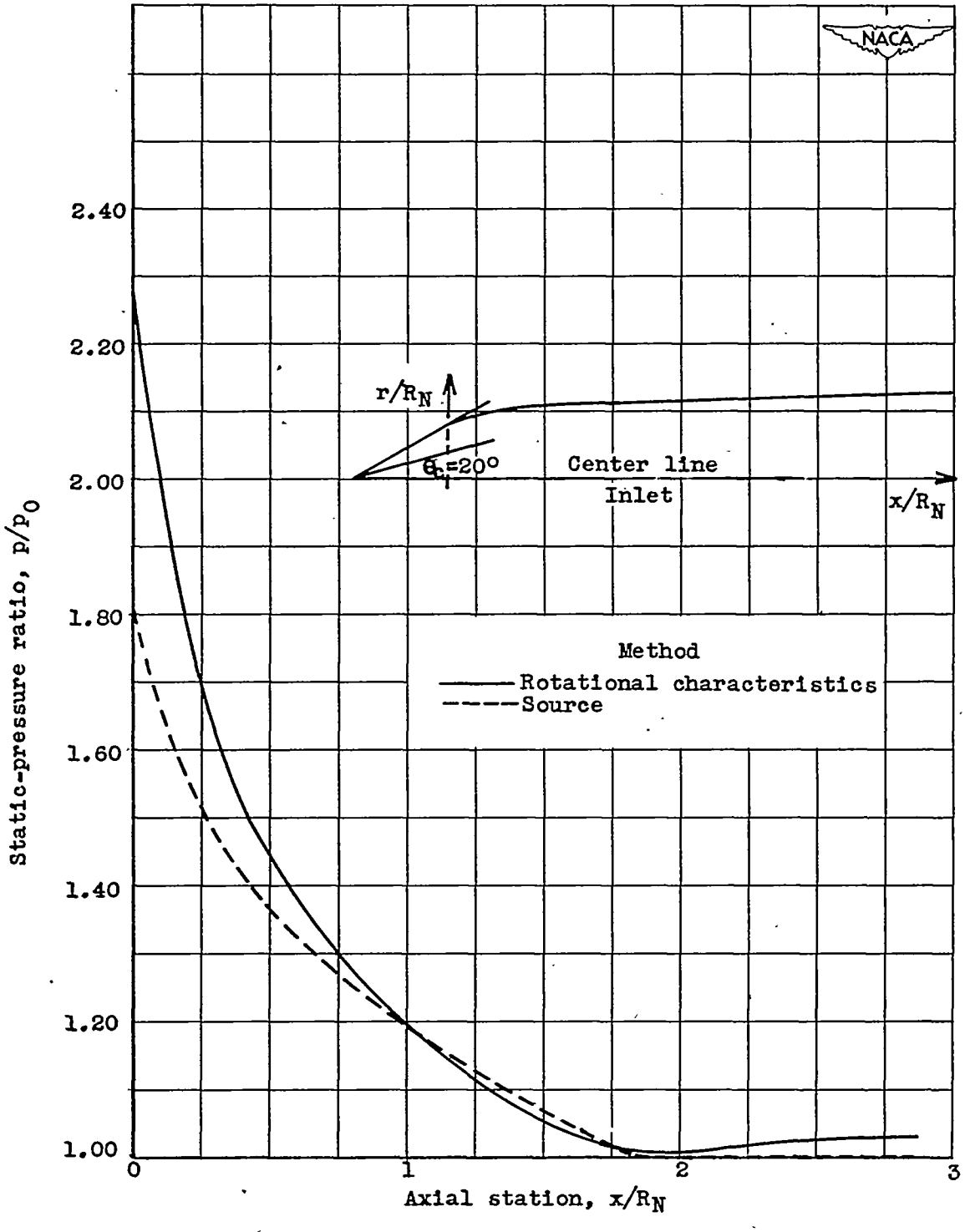

Figure 17. - Comparison of pressure distributions obtained by source method and by exact method of characteristics. Free-stream Mach number, 1.8; area ratio, 0.490; fineness ratio, 4.0.

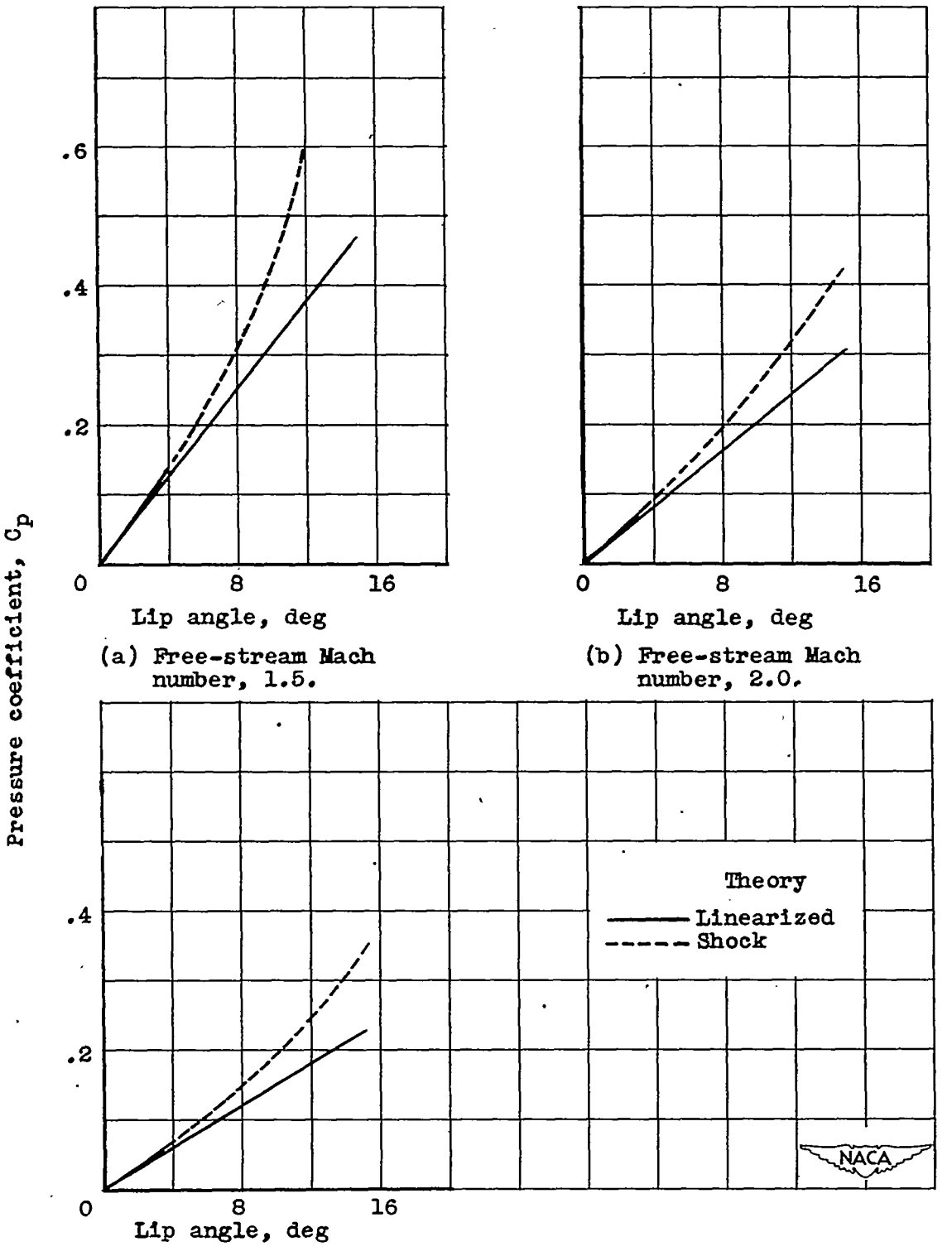

(a) Free-stream Mach number, 1.5.

(b) Free-stream Mach number, 2.0.

(c) Free-stream Mach number, 2.5.

Figure 18. - Lip-pressure coefficient as function of lip angle.

NACA-Langley - 6-12-50 -1050